

Dual Energy CT Attenuation Correction Methods for Quantitative Assessment of Response to Cancer Therapy with PET/CT Imaging

www.tcrt.org

We hypothesize that improved quantification for PET imaging of high atomic number materials can be achieved by combining low-dose x-ray imaging with dual energy CT for PET attenuation correction. Improved quantification of tracer uptake will lead to improved patient outcomes by providing more accurate information for therapeutic choices. Accurate PET/CT measurements of early response will be critical in determining the best cancer therapy option for each patient in a timely manner and in sparing patients the morbidity and cost of ineffective treatments. We first evaluate the potential errors in PET images arising from CT-based attenuation correction when iodine-based contrast is incorrectly classified as bone when forming the linear attenuation coefficient image. We then investigate two methods of reducing errors in the linear attenuation image: an approximate, but fast, hybrid classification/scaling algorithm and a model-based dual-energy CT method that incorporates the polyenergetic spectrum and a noise model in an iterative reconstruction method. Both methods are shown to reduce errors in the estimated linear attenuation coefficient image, but require further study to determine the effects of noise propagation if low-dose CT scans are used for the estimation of the linear attenuation image.

Introduction

Positron emission tomography (PET) radiotracer imaging with the labeled glucose analog 18F-fluorodeoxyglucose (FDG) is being used increasingly in oncology imaging due to its usefulness in detecting and staging cancer and metastatic disease (1-4). A promising application of PET is tumor imaging with newly developed tracers for therapy monitoring with proliferation and apoptosis markers and definition of the tumor environment throughout therapy, constituting a strong basis for an individually tailored therapy for tumor patients (5-9).

The advent of the dual modality PET/CT scanner (14) has significantly enhanced the physician's armamentarium for the diagnosis and staging of cancer as well as for therapy planning and monitoring response to therapy. PET/CT has become the most comprehensive diagnostic tool in oncology imaging by providing improved lesion identification and localization (15). Estimates of the numbers of FDG PET scans performed in the U.S. are shown in Figure 1, which also indicates the rapid saturation by PET/CT systems of the new PET scanner sales market.

The primary purpose of combining CT and PET systems in a single scanner is the precise anatomical localization of regions identified on the PET tracer uptake images (16, 17). Although it is possible to use non-rigid image registration to align separately-acquired whole-body PET and CT images, challenges

Paul E. Kinahan, Ph.D.^{1,*}
Adam M. Alessio, Ph.D.¹
Jeffrey A. Fessler, Ph.D.²

¹Department of Radiology
University of Washington
200 Old Fisheries Center
Box 35 7987
Seattle, WA 98195, USA

²Department of Electrical Engineering
and Computer Science
University of Michigan
4240 EECS Building
1301 Beal Ave.
Ann Arbor, MI 48109, USA

*Corresponding Author:
Paul E. Kinahan, Ph.D.
Email: kinahan@u.washington.edu

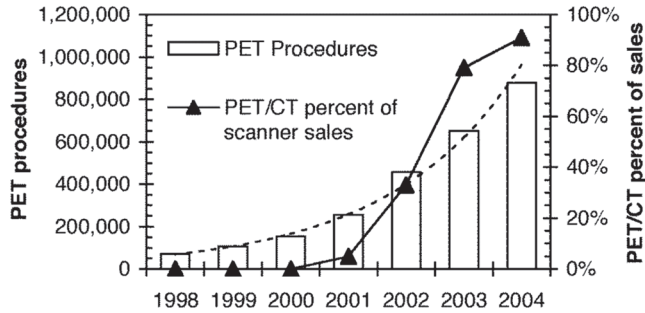


Figure 1: Number of PET procedures per year. The dotted line is an exponential fit ($r^2 = 0.99$) indicating a doubling time of 19 months. Roughly 90% of PET procedures are oncology studies. Also shown is the percentage of new PET or PET/CT scanner sales that are PET/CT scanners (right axis). The total number of PET and PET/CT scanner sales has also been rising: 342 in 2001, 417 in 2002, and 450 in 2003. Data compiled from (10-13).

remain in the practical implementation and validation of software-based methods (18, 19).

Identifying Early Response to Cancer Therapy

A widely used standard for monitoring the effect of cancer therapy on solid tumors is the evaluation of size changes measured from CT images. The Response Evaluation Criteria in Solid

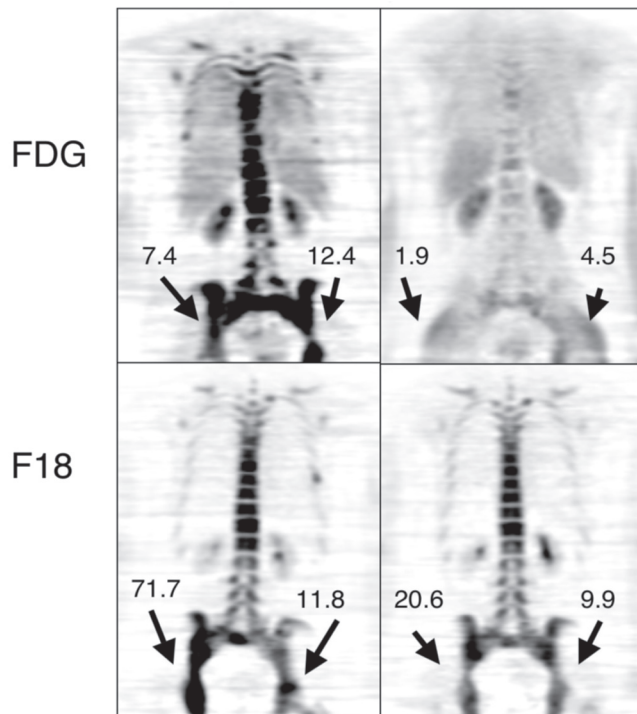


Figure 2: Change in glucose metabolism and fluoride incorporation in bone-dominant metastatic breast cancer. These images demonstrate glucose metabolism (FDG) and bone fluoride incorporation (F18) in a patient with widespread bony metastases from breast cancer before (left) and after hormonal therapy (right). Numbers shown are standardized uptake values (SUVs), a measure of relative tracer uptake. Data courtesy of Dr. David Mankoff, University of Washington.

Tumors (RECIST) standard specifies a ‘positive response’ as a 30% decrease in the maximum diameter (20). This approach has several problems, including the long time lag after therapy (six months or more) necessary for anatomical changes to become evident (21). By then if there is no response, time may have run out for other treatment options for the patient. In addition the patient may have undergone several months of ineffective but toxic therapy. Furthermore, cytostatic agents inhibit tumor growth when successful but may not lead to cell death and reduction in tumor size, in which case tumor size is not a good measure of response (22). While RECIST guidelines provide an important standard for evaluating response, alternative and robust methods of evaluating response by biochemical imaging are needed to improve patient management especially with increasing therapeutic choices (5).

There has been increasing awareness of the value of identifying early response to cancer therapy. On January 10th, 2005, the National Cancer Institute (NCI) sponsored a “Workshop on the Role of FDG-PET in the Evaluation of Therapeutic Response in Cancer”. One of the conclusions from the workshop was that improved quantification is needed, including robust and accurate methods for PET/CT (23). Figure 2 illustrates the use of PET imaging to assess response to therapy. The images demonstrate an excellent response to therapy, which had been underestimated by conventional imaging modalities, including CT and bone scans. Some notable features are: The distribution of bony abnormalities is different between FDG PET and fluoride PET; and response to therapy is qualitatively and quantitatively apparent in the FDG PET image. The qualitative appearance of the fluoride image, however, is relatively stable over the course of treatment, and response to therapy is based largely on quantitative assessment. This emphasizes the need for accurate quantification.

CT-based Attenuation Correction (CTAC)

An important synergy of PET/CT scanners is the use of the CT images for attenuation correction of the PET emission data (24-26). All manufacturers of PET/CT scanners incorporate X-ray CT based attenuation correction (CTAC) algorithms in their systems, and for the majority of PET/CT scanners it is the only option offered (27). This approach offers the significant advantage that the CT data has much lower statistical noise and can be acquired in a shorter time than a standard PET transmission scan (24). CT transmission scans can also be acquired after the PET tracer is injected, allowing the ability to collect unbiased post-injection transmission scans. This reduces image bias from emission contamination while shortening the time spent by a patient on the scanner bed and providing more efficient use of scanner time.

To be used for attenuation correction, the CT data must be transformed to an estimate of the attenuation coefficients at

511 keV. However, there is no unique transformation from CT energies (~30 to 140 keV) to 511 keV due to the possibility of independent variations in density and atomic number (Z) (28). Two materials with different atomic numbers may have similar CT values but different attenuation coefficients at 511 keV. Conversely, it is possible for two distinct materials with the same value of attenuation coefficient at 511 keV to have different CT numbers.

Biases in the CTAC image propagate to errors in the PET image in the same general location (29). Three methods have been considered for converting a CT image to attenuation coefficients at 511 keV: segmentation, scaling, and dual-energy X-ray scans.

Segmentation: Methods can be used to separate the CT image into regions corresponding to different tissue types, which are then replaced with appropriate attenuation coefficients at 511 keV. However, some tissue and bone regions have continuously-varying densities that cannot be accurately represented by a discrete set of segmented values (30). The increased noise of low-dose CTAC scans can result in misclassification of voxels, with incorrect attenuation coefficients being assigned. For these reasons, segmentation methods have not been adopted for CTAC transforms, although they may have some application for the correction of focal accumulations of CT contrast agents (31, 32).

Scaling: It is possible to estimate the attenuation map of the patient at 511 keV simply by multiplying the entire CT image by the ratio of attenuation coefficients of water (representing soft tissues) at the photon energies of CT and PET. For bone, however, linear scaling is a poor approximation, since photoelectric absorption dominates Compton scatter at the lower range of CT energies (33). Blankespoor *et al.* (34) used bilinear scaling to convert CT images to 140 keV for attenuation correction of SPECT data. In this method, different scaling factors (for water and air, and for water and bone, respectively) are used to calculate the attenuation values for CT numbers H for which $-1000 < H < 0$, and for $H > 0$. The bilinear scaling method has been shown to give reasonable results for low- Z biological materials in practice (25, 35, 36). For high- Z materials such as contrast agents there is some disagreement in the literature. Some investigators report no significant errors introduced by high- Z materials when using scaling methods (37), while others have measured quantitative errors (32, 38-42). While in many cases any CTAC errors may not significantly affect diagnostic utility, they may affect decisions or therapies that depend on accurate estimation of tracer uptake in response to therapy.

The errors introduced by high- Z materials can be understood from Figure 3, which illustrates the standard bilinear method used for estimating the linear attenuation coefficient ($\mu(x,y)$

[cm^{-1}]) image at 511 keV from the CT image. Each voxel in the CT image is scaled according to the “bilinear” transform, which has different slopes for air/water and water/bone mixtures, as described above (26). For iodine, the transformation that should be used is illustrated, but, unfortunately, there is no way to discriminate iodine from bone based on the CT voxel value alone. Thus, either voxels containing contrast are incorrectly scaled as bone, or if the iodine curve is used to produce correct results for contrast agent, then voxels containing bone are incorrectly scaled as contrast agent.

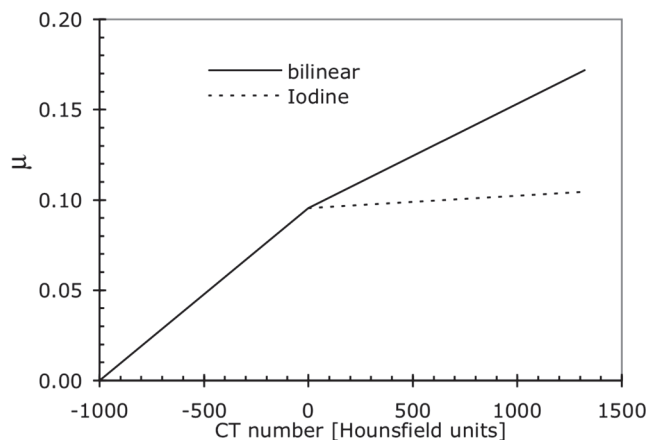


Figure 3: Bilinear scaling factors used to convert CT numbers to linear attenuation coefficients at 511 keV. Also show is the transformation that should be used for iodine-based contrast agents.

Dual Energy X-ray Imaging: A quantitatively accurate estimate of the linear attenuation coefficients at 511 keV can be obtained by collecting two CT scans using X-ray beams with different energy spectra and by estimating the energy dependence of attenuation coefficients in terms of a Compton scattering component and a photoelectric absorption component (43, 44), or by other material bases. The separate component images can then be combined to synthesize an accurate image of attenuation coefficients at any energy. Numerous medical applications of dual-energy imaging, such as bone mineral density measurements (45), as well as non-medical applications have been explored (46). Dual-energy CTAC would allow for accurate attenuation correction in PET/CT imaging that involves high- Z materials, including bone, contrast, and metals. This approach was used to form a monoenergetic attenuation map at 140 keV by Hasegawa *et al.* for a prototype SPECT/CT detector block (47) and for separate SPECT and CT scans by Guy *et al.* (48). A drawback of the dual-energy CT method is that the inverse problem of estimating the component sinograms is poorly conditioned (49), leading to excessive noise amplification. To make dual-energy CTAC feasible for PET/CT imaging, additional steps are needed to reduce noise in the estimated attenuation image at 511 keV. Image reconstruction algorithms that model the acquisition physics can reduce statistical noise in

DECT. There have, however, been very few iterative image reconstruction algorithms proposed for DECT. Sukovic and Clinthorne have investigated iterative algorithms for dual-energy CT reconstruction based on a weighted least-squares approach assuming *monoenergetic* scans (50). We describe below a *polyenergetic* version of the Sukovic and Clinthorne weighted least-squares algorithm for CTAC estimation appropriate for PET/CT scanners (51, 52), and evaluate its usefulness for dual energy CTAC. We call this method the dual-energy weighted least-squares algorithm (DE-WLS).

We also investigate an approximate dual-energy method (called hybrid DECTAC) that allows discrimination of contrast from bone (53, 54). This allows the selection of correct scaling factors for bone versus contrast, but not necessarily other materials. Recently Bacharach *et al.* described the same approach (55). Watson *et al.* described a related method (56) that used dual-energy CT to correctly estimate bone linear attenuation values.

We first evaluate the potential errors in PET images arising from CT-based attenuation correction when contrast is incorrectly classified as bone in the estimation of the linear attenuation coefficient image. We then investigate the two methods described above for reducing errors in the linear attenuation image: the approximate, but fast, hybrid classification/scaling algorithm and the model-based dual-energy CT method that incorporates the polyenergetic spectrum, and a noise model in an iterative reconstruction method.

Materials and Methods

Impact of Errors from Contrast Agent Enhancement

We first investigate the bias introduced by incorrect estimation of linear attenuation coefficients estimated by the standard bi-linear method. This used computer simulations of a abdomen-sized object with a set of six test objects (5 cm diameter regions) of differing standardized uptake val-

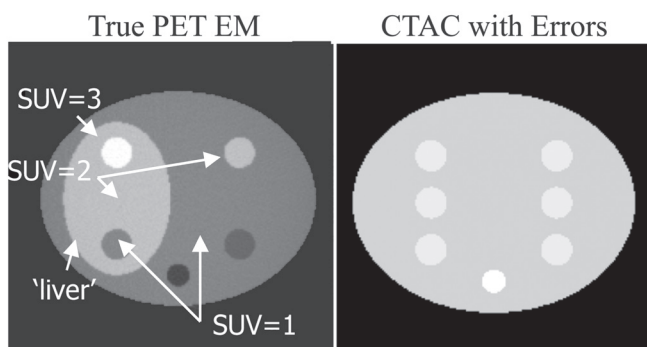


Figure 4: Test objects used for simulation study investigating the propagation of errors from biased attenuation correction factors (CTAC with errors) into the attenuation corrected PET image.

ues (SUVs) with two different local background SUVs as illustrated in Figure 4 (left). The two background regions had SUVs of 1.0 and 2.0, while the test objects had SUVs of 0.5, 1.0, 2.0, and 3.0 as shown. The corresponding attenuation values for the six objects should ideally have the linear attenuation coefficient as background. We simulated the effect of contrast agent being incorrectly scaled as bone, as illustrated in Figure 4 (right). The effect of contrast agent enhancement of 20, 100, and 500 Hounsfield units (HU) were evaluated for each SUV of the test objects.

Method 1: Hybrid Dual-Energy CTAC (DECTAC)

The proposed dual-energy hybrid method classifies materials based on their changes in CT number from scans at two different kVp, taking advantage of the large differences in the photoelectric cross-sections of iodine and barium versus calcium (57) to determine how to scale each voxel in the CTAC image.

Since bone and contrast values span a wide range of CT values, we have derived a classification scheme for the CT difference images (*e.g.*, 80 and 140 kVp) by simply using the midpoint of the relative change in CT numbers, in other words the HU difference depends on the HU value to account for variable concentrations of contrast and variable bone density (Fig. 5) (53). When the correct material (bone or contrast) is determined, then the appropriate scaling factor from Figure 3 is applied to the corresponding voxel in the first CT image.

To test this approach, we acquired CT measurements at 80, 100, 120, and 140 kVp of a 20 cm diameter test phantom containing water and 5 cm diameter cylinders of air, dilute iodine-based contrast agent and CaCl_2 in solution (bone equivalent atomic number). The resulting CT numbers were evaluated at each tube voltage. The standard bilinear CT scaling method and the hybrid method were applied to

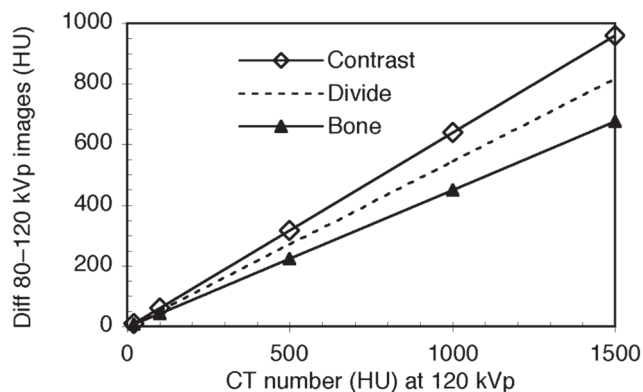


Figure 5: DE-CTAC Classification scheme. Contrast versus bone discrimination is accomplished by determining if the change in CT number is greater than a threshold, which depends on the CT number for one of the kVp images.

the 140 kVp CT image. A standard PET transmission scan was also acquired for reference.

Method 2: Dual-Energy Weighted Least-squares Algorithm (DE-WLS)

The above Hybrid DE-CTAC hybrid scheme will help discriminate contrast from bone, but will not suffice if unknown or multiple high-Z materials are present. We have implemented a new PWLS algorithm for dual energy CT similar to that of Sukovic and Clinthorne (50), but with a polyenergetic model of the spectrum, rather than their monoenergetic approach (51, 52). We term this the dual-energy weighted least-squares (DE-WLS) algorithm. To derive the algorithm we start with a parameterization that uses basis functions that are each separable in space and energy $\mu(\vec{x}, E) = \sum_{l=1, L} \sum_{j=1, N_p} \beta_l(E) b_j(\vec{x}) x_{lj}$, where $\beta_l(E)$ is the mass attenuation of the l th material type, $b_j(\vec{x})$ are spatial basis functions, and x_{lj} are the desired coefficients for material l and voxel j . Thus, the spatially-varying density of each material is given by $\rho_l(\vec{x}) = \sum_j b_j(\vec{x}) x_{lj}$ and the system model is given by $a_{ij} = \int_{L_i} b_j(\vec{x}) d\ell$, where L_i denotes the i th line of response (LOR). The material basis sinograms are then given by

$$s_{il}(\mathbf{x}) \triangleq \int_{L_i} \rho_l(\vec{x}) d\ell = \sum_{j=1, N_p} a_{ij} x_{lj}$$

To solve for \mathbf{x} , we use the PWLS criterion: $\mathbf{x} = \arg \min \Psi(\mathbf{x})$, with $\Psi(\mathbf{x}) \triangleq \sum_{i=1}^{N_D} (\hat{s}_i - \mathbf{s}_i(\mathbf{x}))' \mathbf{W}_i (\hat{s}_i - \mathbf{s}_i(\mathbf{x})) + R(\mathbf{x})$, where N_D is the number of lines of response, and \hat{s}_i are the material basis sinograms estimated from the CT sinograms using standard dual-energy decomposition methods, and \mathbf{W}_i are the inverse variances of \hat{s}_i . The function $R(\mathbf{x})$ is a regularizer that controls noise.

We tested the DE-WLS approach with simulated and measured data. For the simulations we used a 20 cm diameter phantom containing three smaller 5 cm diameter cylinders comprised of (i) air, (ii) half soft tissue and half bone with a total density of 1.5 g/cm³; and (iii) a bone cylinder with a total density of 2 g/cm³. The large background cylinder was all soft tissue component with a density of 1 g/cm³. The attenuation coefficients at 511 keV were estimated by (i) standard bilinear scaling, (ii) dual energy CT with a standard dual-energy decomposition method followed by filtered backprojection (FBP) and the DE-WLS algorithm.

Results

Impact of Errors from Contrast Agent Enhancement

Figure 6 illustrates the effects of biases from CT-based attenuation correction for noiseless PET simulations. The difference image between the true PET image (Fig. 4) and the reconstructed image is also shown. The errors, expressed as

standardized uptake values (SUV), are plotted in Figure 7 as a function of the SUV of the test object for the different levels of contrast-induced CT number errors.

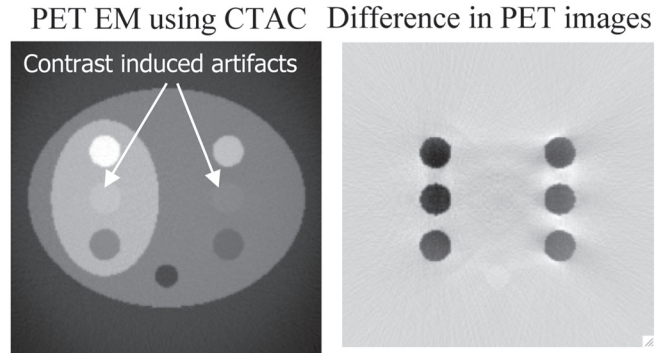


Figure 6: Noiseless simulation study showing propagation of errors from biased attenuation correction factors into the attenuation corrected PET image (PET EM using CTAC). A difference image from the true PET image (Fig. 4) shows that both quantitative errors and complex artifacts can occur.

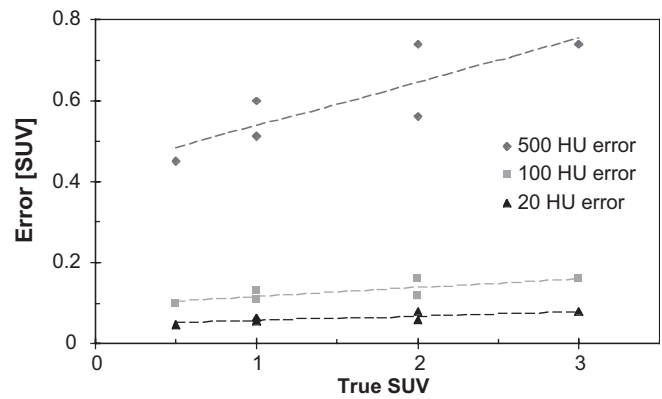


Figure 7: Results of simulation study showing propagation of CT error of different Hounsfield units (HU) into the error in the attenuation corrected PET standard uptake values (SUV).

Method 1: Hybrid Dual-Energy CTAC (DECTAC)

For the measured phantom data there was essentially no variation in CT number for air or water with tube voltage. For the CaCl₂ solution the CT numbers increased from 546 to 897 HU, while the dilute contrast agent values increased from 856 to 1721 HU as the tube voltage was dropped from 140 to 80 kVp. Thus, starting from a standard CT scan at 120 kVp, a second (low-dose) CT scan at 80 kVp would show a difference of ~400 HU between contrast agents and CaCl₂ (bone equivalent). This is similar to heuristic bone-imaging procedures for CT. One of the dual-energy difference images is shown in Figure 8, which shows that there is no variation in CT number with kVp for both air and water, while there are differing variations for bone and contrast agent. The difference image is sensitive to the photoelectric absorption, which is higher in iodine-based contrast agent than in bone.

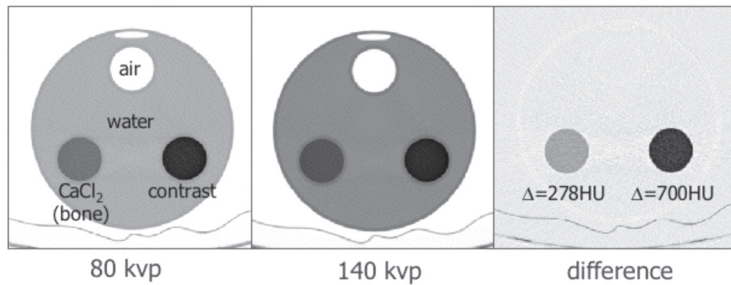


Figure 8: Measured 20 cm diameter water cylinder with 5 cm cylindrical inserts containing air, bone-equivalent solution of CaCl_2 and dilute iodine-based contrast agent scanned at two different kVp.

By classifying the voxels in the CT image (Fig. 8) based on the scheme illustrated in Figure 5, the correct scaling factors for bone and contrast agent (Fig. 3) can be used to convert the CT image to an estimate of the linear attenuation coefficients at 511 keV. This was evaluated as shown in Figure 9 for the same test phantom used in Figure 8. The bilinear method has a substantial error for the 5 cm diameter contrast agent filled region, when compared to the measured PET transmission scan at 511 keV. This error is reduced from -38% to +6% with the use of the dual energy hybrid/bilinear method.

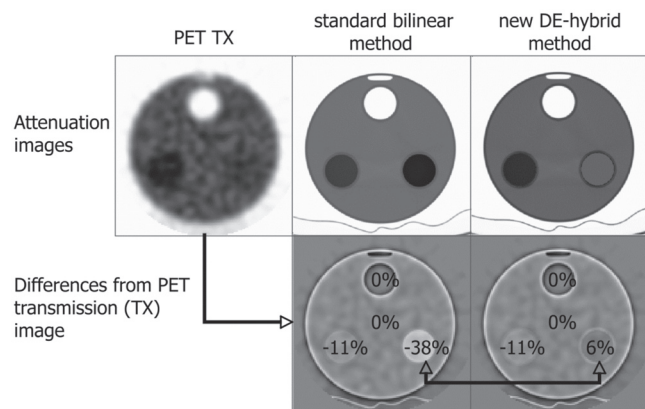


Figure 9: Effect of bilinear and hybrid scaling methods on measured data, compared to measured PET transmission scan (TX).

Method 2: Dual-Energy Weighted Least-squares Algorithm (DE-WLS)

Results of the simulation studies are shown in Figure 10. The CT-based attenuation images were scaled to 511 keV by either bilinear scaling or dual energy CT. The dual-energy CT images were reconstructed with both FBP and the DE-WLS algorithms. Also shown (bottom) are the differences from the true values at 511 keV. There is a significant reduction of bias using DECT (from 20% to ~0% for the tissue/bone mixture) compared to bilinear scaling. The FBP image, however, has high levels of statistical noise, as expected. These noise levels are reduced from ~8% to ~3% by the use of our DE-WLS algorithm. Within the object RMS errors decrease

from 11% using bi-linear scaling to 9% with DE-FBP and to 7.5% with DE-WLS.

The computation time of the DE-WLS (with ten iterations) and FBP methods are shown in Figure 11 for a standard workstation. There is a significant increase in computation time required for the DE-WLS, which would render it infeasible for clinical implementation with standard 512×512 CT images. For attenuation correction of PET data, however, only 128×128 (or perhaps even 64×64) images are needed, for relatively thick slices, which reduces the DE-WLS computation time down to clinically feasible levels.

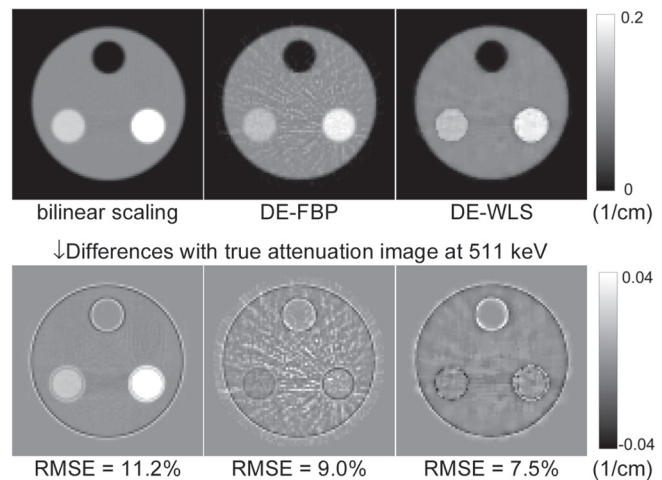


Figure 10: Comparison of CT-based attenuation images scaled to 511 keV by either bilinear scaling or dual energy CT. Also shown (bottom row) are the differences from the true values at 511 keV.

Discussion

Currently, CT attenuation correction has the potential for significant bias in the attenuation correction factors. We present results showing the propagation of these errors into

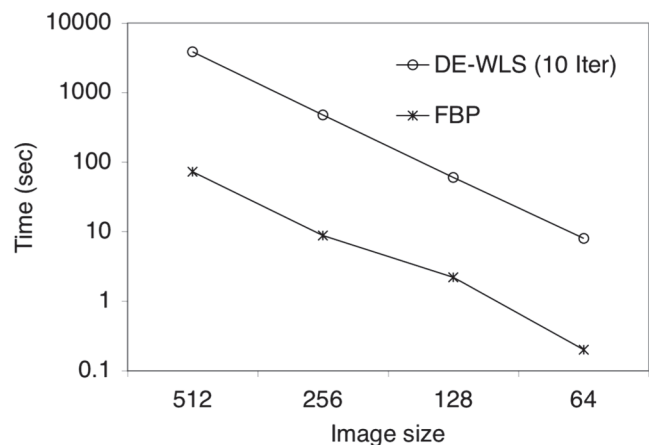


Figure 11: Computation time for the DE-WLS and FBP algorithms as a function of image size when implemented on a standard workstation.

attenuation corrected PET images. Dual energy CT-based attenuation correction offers the potential of reducing bias in the CTAC image and, thus, can also reduce bias in the final PET emission image.

Dual energy CT attenuation correction results in increased noise in reconstructions from the basis material decomposition process and from the potential use of low-dose CT. Noise from dual energy CT imaging can be reduced through the use of: (i) a statistically principled reconstruction method, (ii) a coarse reconstruction grid, and (iii) only the summed component image at 511keV.

Both the simulated and measured phantom results demonstrate the feasibility of using dual-energy CTAC for accurate attenuation correction in PET/CT oncology imaging. We have shown that with the dual-energy hybrid method it is possible to discriminate contrast versus bone in the CTAC images and apply the correct scale factor for accurate calibration and attenuation correction. We note that this method may not be suitable for standard 512×512 high resolution CT images due to patient motion or noise amplification. However, for low-resolution 128×128 (or even 64×64) CTAC images reconstructed with statistically-principled algorithms we expect that the noise amplification will be acceptable.

We also evaluated a polychromatic DE-PWLS iterative reconstruction method that is potentially more accurate than the dual-energy hybrid method. We showed that the reduction of the CTAC sinograms and image matrix sizes to 128×128 or 64×64 leads to iterative reconstructions of dual energy CT component images in a clinically feasible amount of time.

In addition to errors from scaling the CTAC image to 511 keV described above, three other sources of error from CT-based attenuation have been recognized (14, 26): CT field of view truncation artifacts; CT beam hardening; and respiratory motion mismatch between the PET and CT acquisitions. An ameliorating factor for truncation artifacts is that missing attenuation correction factors can be closely approximated from the truncated projection data, leading to accurate CTAC images (58). We also note that beam hardening effects are minimized by the use of a dual energy CT method. Research in compensating for respiratory motion are ongoing.

There is a clear consensus that PET/CT imaging has significant potential as biomarker for assessing response to therapy. Recent recommendations for such PET imaging protocols have been announced by the National Cancer Institute (23). In addition the Cancer Imaging Program at NCI is sponsoring the development of a database of CT and PET/CT images pre- and post-therapy as a testing ground for determining if there has been a response to therapy, by using anatomical and/or functional information (59). This RIDER (Refer-

ence Image Database to Evaluate Response) database is intended to enable industry and academia to develop, test, and compare semi-automated and automated software tools for change analysis in response to therapy. A key initial step towards this project is a consensus on procedures for obtaining quantitatively accurate PET images from PET/CT scanners.

Conclusion

We presented two successful DECT strategies for reducing quantitative errors from CT-based attenuation correction. The quantitative biases present in PET/CT imaging clearly do not prevent its effective use in the diagnosis and staging of cancer. However, a key component of the use of PET in the management of cancer will be for evaluating response to therapy and for making therapeutic choices. These applications require the use of quantitative PET/CT imaging to assure they have a positive impact on patient management. Accurate PET/CT measurements of early response will be critical in determining the best cancer therapy option for each patient in a timely manner and in sparing patients the morbidity and cost of ineffective treatments.

Acknowledgements

We would like to acknowledge helpful discussion with Drs. David Mankoff and Hubert Vesselle in the Department of Radiology at the University of Washington, and Drs Barbara Croft and Lawrence Clarke in the Cancer Imaging Program of the National Cancer Institute. This work was supported by NCI Grants R01-CA74135 and R01-CA115870.

References

1. Wahl, R. L. Clinical Oncology Update: The Emerging Role of Positron Emission Tomography: Part I. *Principal and Practice of Oncology Updates 11*, 1-18 (1997).
2. Weber, W. A., Avril, N., Schwaiger, M. Relevance of Positron Emission Tomography (PET) in Oncology. *Strahlentherapie und Onkologie 175*, 356-373 (1999).
3. Bomanji, J. B., Costa, D. C., Ell, P. J. Clinical Role of Positron Emission Tomography in Oncology. *Lancet Oncology 2*, 157-164 (2001).
4. Rohren, E. M., Turkington, T. G., Coleman, R. E. Clinical Applications of PET in Oncology. *Radiology 231*, 305-332 (2004).
5. Krohn, K. A., Mankoff, D. A., Eary, J. F. Imaging Cellular Proliferation as a Measure of Response to Therapy. *Journal of Clinical Pharmacology Suppl.* 96S-103S (2001).
6. Mankoff, D. A., Muzi, M., Krohn, K. A. Quantitative Positron Emission Tomography Imaging to Measure Tumor Response to Therapy: What is the Best Method? *Molecular Imaging & Biology 5*, 281-285 (2003).
7. Cohade, C., Wahl, R. L. PET Scanning and Measuring the Impact of Treatment. *Cancer J 8*, 119-134 (2002).
8. Stahl, A. *et al.* Positron Emission Tomography as a Tool for Translational Research in Oncology. *Molecular Imaging in Biology 6*, 214-224 (2004).
9. Juweid, M. E., Cheson, B. D. Positron-emission Tomography and Assessment of Cancer Therapy. *N. Engl. J. Med.* 354, 496-507 (2006).
10. Burns, M. PET Market Appears Poised for Continued Strong Growth. *Diagnostic Imaging* (2003).

11. Ridley, E. L. PET/CT Growth Sparks Gains in U.S. PET Market. AuntMinnie.com (2003).
12. Staff. PET Usage Surges in 2002. AuntMinnie.com (2003).
13. Staff. PET Procedure Volume to Surge. AuntMinnie.com (2004).
14. Beyer, T. et al. A Combined PET/CT Scanner for Clinical Oncology. *Journal of Nuclear Medicine* 41, 1369-1379 (2000).
15. Czernin, J. Summary of Selected PET/CT Abstracts from the 2003 Society of Nuclear Medicine Annual Meeting. *Journal of Nuclear Medicine* 45, 102S-103S (2004).
16. Wahl, R. L. et al. "Anatomometabolic" Tumor Imaging: Fusion of FDG PET with CT or MRI to Localize Foci of Increased Activity. *J. Nucl. Med.* 34, 1190-1197 (1993).
17. Townsend, D. W., Beyer, T., Blodgett, T. M. PET/CT Scanners: A Hardware Approach to Image Fusion. *Semin. Nucl. Med.* 33, 193-204 (2003).
18. Slomka, P. J. Software Approach to Merging Molecular with Anatomic Information. *J. Nucl. Med.* 45 Suppl. 1, 36S-45S (2004).
19. Wahl, R. L. Why Nearly All PET of Abdominal and Pelvic Cancers will be Performed as PET/CT. *Journal of Nuclear Medicine* 45, 82S-95S (2004).
20. Therasse, P. et al. New Guidelines to Evaluate the Response to Treatment in Solid Tumors. European Organization for Research and Treatment of Cancer, National Cancer Institute of the United States, National Cancer Institute of Canada. *J. Natl. Cancer Inst.* 92, 205-216 (2000).
21. Husband, J. E. et al. Evaluation of the Response to Treatment of Solid Tumours – A Consensus Statement of the International Cancer Imaging Society. *Br. J. Cancer* 90, 2256-2260 (2004).
22. Michaelis, L. C., Ratain, M. J. Measuring Response in a Post-RECIST World: From Black and White to Shades of Grey. *Nat. Rev. Cancer* 6, 409-414 (2006).
23. Shankar, L. K. et al. Consensus Recommendations for the Use of 18F-FDG PET as an Indicator of Therapeutic Response in Patients in National Cancer Institute Trials. *J. Nucl. Med.* 47, 1059-1066 (2006).
24. Kinahan, P. E., Townsend, D. W., Beyer, T., Sashin, D. Attenuation Correction for a Combined 3D PET/CT Scanner. *Med. Phys.* 25, 2046-2253. (1998).
25. Burger, C. et al. PET Attenuation Coefficients from CT Images: Experimental Evaluation of the Transformation of CT into PET 511-keV Attenuation Coefficients. *Eur. J. Nucl. Med. Mol. Imaging* 29, 922-997. (2002).
26. Kinahan, P. E., Hasegawa, B. H., Beyer, T. X-ray Based Attenuation Correction for PET/CT Scanners. *Seminars in Nuclear Medicine* 33, 166-179 (2003).
27. Alessio, A., Kinahan, P. E., Cheng, P., Vesselle, H., Karp, J. S. PET/CT Scanner Instrumentation, Challenges, and Solutions. *Radiologic Clinics of North America* 42, 1017-1032 (2004).
28. Schneider, W., Bortfeld, T., Schlegel, W. Correlation Between CT Numbers and Tissue Parameters Needed for Monte Carlo Simulations of Clinical Dose Distributions. *Physics in Medicine and Biology* 45, 459-478 (2000).
29. Bai, C. Y. et al. An Analytic Study of the Effects of Attenuation on Tumor Detection in Whole-body PET Oncology Imaging. *Journal of Nuclear Medicine* 44, 1855-1861 (2003).
30. Robinson, P. J., Kreef, L. Pulmonary Tissue Attenuation with Computed Tomography: Comparison of Inspiration and Expiration Scans. *Journal of Computer Assisted Tomography* 3, 740-748 (1979).
31. Carney, J., Beyer, T., Brasse, D., Yap, J. T., Townsend, D. W. CT-Based Attenuation Correction for PET/CT Scanners in the Presence of Contrast Agent. *IEEE Nuclear Science Symposium and Medical Imaging Conference* (2002).
32. Nehmeh, S. A. et al. Correction for Oral Contrast Artifacts in CT Attenuation-corrected PET Images Obtained by Combined PET/CT. *Journal of Nuclear Medicine* 44, 1940-1944 (2003).
33. LaCroix, K. J., Tsui, B. M. W., Hasegawa, B. H., Brown, J. K. Investigation of the Use of X-ray CT Images for Attenuation Compensation in SPECT. *IEEE Transactions on Nuclear Science NS-41*, 2793-2799 (1994).
34. Blankespoor, S. C. et al. Attenuation Correction of SPECT Using X-Ray CT on an Emission-Transmission CT System: Myocardial Perfusion Assessment. *IEEE Transactions on Nuclear Science* 43, 2263-2274 (1996).
35. Kamel, E. et al. CT vs 68Ge Attenuation Correction in a Combined PET/CT System: Evaluation of the Effect of Lowering the CT Tube Current. *Eur. J. Nucl. Med. Mol. Imaging* 29, 346-50. (2002).
36. Nakamoto, Y. et al. PET/CT: Comparison of Quantitative Tracer Uptake Between Germanium and CT Transmission Attenuation-corrected Images. *J. Nucl. Med.* 43, 1137-143. (2002).
37. Dizendorf, E., Hany, T. F., Buck, A., von Schulthess, G. K., Burger, C. Cause and Magnitude of the Error Induced by Oral CT Contrast Agent in CT-based Attenuation Correction of PET Emission Studies. *Journal of Nuclear Medicine* 44, 732-738 (2003).
38. Antoch, G. et al. Effect of Oral Contrast Agents on Computed Tomography-based Positron Emission Tomography Attenuation Correction in Dual-modality Positron Emission Tomography/Computed Tomography Imaging. *Investigative Radiology* 38, 784-789 (2003).
39. Bujenovic, S., Manning, F., Chakrabarti, R., Ladnier, D. Artifactual 2-deoxy-2-[(18)F]fluoro-D-glucose Localization Surrounding Metallic Objects in a PET/CT Scanner using CT-based Attenuation Correction. *Mol. Imaging Biol.* 5, 20-22 (2003).
40. Goerres, G. W., Ziegler, S. I., Burger, C., von Schulthess, T., Buck, A. Artifacts at PET and PET/CT Caused by Metallic Hip Prosthetic Material. *Radiology* 226, 577-584 (2003).
41. Nakamoto, Y. et al. Effects of Nonionic Intravenous Contrast Agents at PET/CT Imaging: Phantom and Canine Studies. *Radiology* 227, 817-824 (2003).
42. Visvikis, D. et al. CT-based Attenuation Correction in the Calculation of Semi-quantitative Indices of F-18 FDG Uptake in PET. *European Journal of Nuclear Medicine and Molecular Imaging* 30, 344-353 (2003).
43. Alvarez, R., Seppi, E. Comparison of Noise and Dose in Conventional and Energy Selective Computed-Tomography. *IEEE Transactions on Nuclear Science* 26, 2853-2855 (1979).
44. Alvarez, R. E., Macovski, A. Energy-Selective Reconstructions in X-Ray Computerized Tomography. *Physics in Medicine and Biology* 21, 733-744 (1976).
45. Greenfield, M. A. Current Status of Physical Measurements of the Skeleton. *Medical Physics* 19, 1349-1357 (1992).
46. Engler, P., Friedman, W. D. Review of Dual-Energy Computed-Tomography Techniques. *Materials Evaluation* 48, 623-629 (1990).
47. Hasegawa, B. H. et al. Object Specific Attenuation Correction of SPECT with Correlated Dual-energy X-ray CT. *IEEE Transactions on Nuclear Science NS-40*, 1242-1252 (1993).
48. Guy, M. J. et al. DETECT – Dual Energy Transmission Estimation CT – For Improved Attenuation Correction in SPECT and PET. *IEEE Transactions on Nuclear Science* 45, 1261-1267 (1998).
49. Kalender, W. A., Klotz, E., Kostaridou, L. An Algorithm for Noise Suppression in Dual Energy CT Material Density Images. *IEEE Transactions on Medical Imaging* 7, 218-224 (1988).
50. Sukovic, P., Clinthorne, N. H. Penalized Weighted Least-squares Image Reconstruction for Dual Energy X-ray Transmission Tomography. *IEEE Transactions on Medical Imaging* 19, 1075-1081 (2000).
51. Fessler, J. A., Elbakri, I. A., Sukovic, P., Clinthorne, N. H. Maximum-likelihood Dual-energy Tomographic Image Reconstruction. *Medical Imaging 2002: Image Processing* 4684, 38-49 (2002).
52. Kinahan, P. E., Fessler, J. A., Alessio, A. M., Lewellen, T. K. Quantitative Attenuation Correction for PET/CT Using Iterative Reconstruction of Low-dose Dual-energy CT. *Nuclear Science Symposium Conference Record, 2004 IEEE Nuclear Science Symposium Conference Record, 2004 IEEE* 5, 3285-3289 Vol. 5 (2004).

53. Kinahan, P. E. *et al.* Dual-Energy CT For Quantitative Attenuation Correction in PET/CT Imaging. *2004 RSNA* (abstract) (2004).
54. Kinahan, P. E., Alessio, A. M., Fessler, J. A., Lewellen, T. K., Veselle, H. A Simple Dual Energy Method for CT-Based Attenuation Correction that Accounts for Contrast Agents in PET/CT Imaging. *Journal of Nuclear Medicine* 46, 113P (abstract) (2005).
55. Bacharach, S. L., Freedman, N. M. T., Maass-Moreno, R., Le Meunier, L. Dual Energy CT for Detecting Contrast Media in PET/CT. *Journal of Nuclear Medicine* 46, 168P (abstract) (2005).
56. Watson, C. C., Rappoport, V., Faul, D., Townsend, D. W., Carney, J. P. A Method for Calibrating the CT-based Attenuation Correction of PET in Human Tissue. *Nuclear Science, IEEE Transactions on Nuclear Science, IEEE Transactions on* 53, 102-107 (2006).
57. Hubbell, J. H., Seltzer, S. M. Tables of X-Ray Mass Attenuation Coefficients and Mass Energy-Absorption Coefficients. **JOURNAL?!** January, 2003, (1997).
58. Hsieh, J. *et al.* Algorithm to Extend Reconstruction Field-of-View. *2004 IEEE International Symposium on Biomedical Imaging* 1404-1407 (2004).
59. Clarke, L. P. *et al.* Building of Large Public Databases For Validation of Software Tools. *Sixth National Forum on Biomedical Imaging in Oncology* (2005).

Received: April 21, 2006; Revised: July 2, 2006;

Accepted: July 5, 2006